Low-Temperature Solution-Phase Synthesis of NiAu Alloy Nanoparticles via Butyllithium Reduction: Influences of Synthesis Details and Application As the Precursor to Active Au-NiO/S...

ARTICLE *in* THE JOURNAL OF PHYSICAL CHEMISTRY C · APRIL 2009

Impact Factor: 4.77 · DOI: 10.1021/jp811411y

7 AUTHORS, INCLUDING:

Zhen Ma
Fudan University
98 PUBLICATIONS **2,201** CITATIONS

SEE PROFILE

Low-Temperature Solution-Phase Synthesis of NiAu Alloy Nanoparticles via Butyllithium Reduction: Influences of Synthesis Details and Application As the Precursor to Active Au-NiO/SiO_2 Catalysts through Proper Pretreatment

Shenghu Zhou,[†,‡] Zhen Ma,[†] Hongfeng Yin,[†] Zili Wu,[†] Bryan Eichhorn,[§] Steven H. Overbury,[†] and Sheng Dai*[,†]

Center for Nanophase Materials Science and Chemical Sciences Division, Oak Ridge National Laboratory, Oak Ridge, Tennessee 37831, The Institute for Advanced Materials & Nano Biomedicine, Tongji University, Shanghai 200092, P. R. China, and Department of Chemistry and Biochemistry, University of Maryland, College Park, Maryland 20742

Received: December 25, 2008; Revised Manuscript Received: February 8, 2009

Bimetallic nanoparticles (NPs) have wide applications in electronics, photonics, and catalysis. However, it is particularly challenging to synthesize size-controllable alloy nanoparticles (e.g., NiAu) with bulk immiscible metals as the components. Here we report the synthesis of isolable NiAu alloy nanoparticles with tunable and relatively uniform sizes via a coreduction method employing butyllithium as the reducing agent and trioctylphosphine as the protecting agent. The influences of synthesis conditions (e.g., protecting agent, aging temperature, and the solvent used to wash the product) were investigated, and the synthesis mechanism was preliminarily surveyed. The NiAu alloy nanoparticles obtained were then used as the precursor to prepare an Au−NiO/SiO_2 catalyst highly active in low-temperature CO oxidation, and the effects of pretreatment details and catalyst compositions on catalytic activity were studied. Relevant characterization employing XRD, TEM, UV−vis, TG/DTG, and FT-IR was conducted. In addition, the importance of the current synthesis of NiAu alloy NPs and the contribution of the catalyst design were discussed in the context of the literature.

1. Introduction

The synthesis of bimetallic nanoparticles (NPs) with well-defined architectures (e.g., core−shell structures,[1−7] heterodimers,[8] alloys[9−12]) has attracted much attention because these materials have unique physicochemical properties and are useful in electronics, photonics, and catalysis. Among these architectures, alloy NPs have been the most commonly investigated owing to their tailored activity and selectivity in catalytic reactions.[11−14] So far, most work in the literature has focused on the synthesis of alloy NPs made from bulk miscible metals (e.g., PtPd), but the synthesis of alloy NPs with bulk immiscible metals (e.g., NiAu) represents a significant challenge.[15]

Traditional bimetallic NiAu catalysts are effective in a few catalytic reactions such as steam-reforming[16−18] and hydrodechlorination.[19] Theoretical calculation suggested that the preferred stable structure is an Ni@Au core−shell structure where Au atoms are very present at the surface of small Ni particles, mainly at the low-index planes such as (110) facets.[16] Surface science studies demonstrated that Au atoms exist at the first layer of single-crystal Ni surface.[20] Recently, Chen and co-workers synthesized Ni@Au core−shell structures by combining reverse microemulsion and redox-transmetalation methods.[5] However, it is significantly difficult to synthesize homogeneous NiAu alloy NPs because bulk Ni and Au have a large immiscibility gap according to their phase diagram,[21,22] and they also have significantly different reduction potentials. Indeed, NiAu alloy catalysts prepared via high-temperature annealing exhibit relatively large aggregates,[19] whereas NiAu alloy NPs prepared via an electrodeposition method are in fact Au-rich alloys with irregular shapes and a relatively big mean particle size (25 nm).[23]

Recently, low-temperature solution methods to synthesize intermetallic compounds and alloys have been developed.[10,24,25] Notably, Schaak and co-workers synthesized Au_xCu_y, AuPd, and M_xPt_y (M = Fe, Co, Cu, Ag, Ni) intermetallic compounds and alloys using reduced nanocomposites as the starting materials.[24] The underlying principle is to exploit the enhanced reactivity of NPs and the nanometer diffusion distances. Zhou et al. synthesized AuPt alloy NPs via a butyllithium reduction method.[12] The rapid reduction by butyllithium instantly coreduces Au and Pt and traps the AuPt alloy phase that otherwise requires high-temperature annealing (above 1100 °C) in a solid-state method. We recently communicated the extension of this butyllithium reduction method[12] to the synthesis of NiAu alloy NPs and used NiAu alloy NPs as the precursor to prepare a highly active Au−NiO/SiO_2 catalyst for CO oxidation.[26] Schaak and co-workers also used this reduction method to prepare intermetallic compounds Au_3Fe, Au_3Co, and Au_3Ni with relatively big particle sizes.[27]

The main part of our previous short communication[26] focused on the in-depth characterization of NiAu alloy NPs and an Au-NiO/SiO_2 catalyst prepared under optimal conditions, whereas the influences of synthesis parameters on the resulting products, the synthesis mechanism, and the critical roles of pretreatment conditions and catalyst compositions in determining catalytic performance, as well as the contribution of the work to the fields of bimetallic materials synthesis and gold catalysis, were not reported or elaborated in detail. Therefore, we expand on these aspects more explicitly in the current paper. There are two

* Corresponding author. E-mail: dais@ornl.gov. Tel.: (865) 576-7307. Fax: (865) 576-5235.
[†] Oak Ridge National Laboratory.
[‡] Tongji University.
[§] University of Maryland.

10.1021/jp811411y CCC: $40.75
Published on Web 03/17/2009

significant aspects of the work described in this paper. First, the synthesis of size-controlled and homogeneous NiAu alloy NPs has been found to be extremely evasive to date.[15] Hence, the low-temperature solution-phase synthesis of NiAu alloy NPs with well-controlled shapes and sizes should be an important progress that may inspire subsequent bimetallic materials synthesis. Second, catalysis by gold nanoparticles has been intensively studied recently,[28−33] but the use of alloy NPs as precursors to design advanced catalysts with multiple components (i.e., active metal, metal oxide modifier/promoter, solid support) and tailored interfacial structures has been rarely reported. Hence, this work may be of interest to both materials scientists and those working in the area of catalyst design.

2. Experimental Section

The synthesis of NiAu alloy NPs was carried out in a standard Schlenk line under N_2, and the procedure was similar to those of AuPt alloy NPs reported by Zhou et al.[12,26] In a typical synthesis, 0.17 mmol $HAuCl_4 \cdot 3H_2O$ (Aldrich, ≥49.0% as Au) and 0.17 mmol $Ni(acac)_2$ (Aldrich, 95%) were codissolved in 10 mL of dioctyl ether (Aldrich, 99%) with 2 mL of oleylamine (Aldrich, 70%) at 40−50 °C. The warm solution was then injected via a syringe into a room-temperature butyllithium solution containing 15 mL of dioctyl ether and 1.2 mL of 2.0 M butyllithium in cyclohexane (Aldrich, 2.0 M in cyclohexane), resulting in the formation of dark brown colloids. The colloids were stirred for 20 min and then heated to 120 °C for 1.5 h. To study the influence of different aging temperatures, the reaction mixture was further heated to 180−260 °C for 1 h. The mixture was cooled down to room temperature, and 1.25 mL of trioctylphosphine (Aldrich, 90%) was injected to protect the colloids. The colloids were diluted by ethanol and centrifuged to obtain particles. The resulting black powder product can be easily redispersed in nonpolar solvents such as hexane and toluene with the addition of a minimal amount of trioctylphosphine (approximately 1 μL of trioctylphosphine for 1 mg of product).

Several samples for control experiments were prepared accordingly. To synthesize Ni_3Au, 0.085 mmol $HAuCl_4 \cdot 3H_2O$ and 0.255 mmol $Ni(acac)_2$ were codissolved in 5 mL of dioctyl ether with 2 mL of oleylamine at 40−50 °C. The warm solution was then injected via a syringe into a room-temperature butyllithium solution containing 10 mL of dioctyl ether and 1.2 mL of 2.0 M butyllithium in cyclohexane, and the other synthetic conditions are the same as those for NiAu alloy NPs. The aging temperature was kept at 210 °C. To synthesize $NiAu_3$, 0.17 mmol $HAuCl_4 \cdot 3H_2O$ and 0.057 mmol $Ni(acac)_2$ were codissolved in 10 mL of dioctyl ether with 1.33 mL of oleylamine at 40−50 °C. The warm solution was then injected via a syringe into a room-temperature butyllithium solution containing 15 mL of dioctyl ether and 1.0 mL of 2.0 M butyllithium in cyclohexane, and the other procedures are the same as those of NiAu synthesis. The synthesis of Au NPs can be found in our previous communication.[26]

The obtained NiAu or Au NP powders were redispersed in hexane, and a calculated amount of SiO_2 (Cab-O-Sil, surface area of 175 m^2/g) was then added. To be consistent, the Au loading of all the supported catalysts was fixed at 2 wt %. A black powder catalyst was obtained by slightly heating the slurry under N_2 to remove hexane, followed by vacuum drying overnight. The above catalyst was washed with acetone and ethanol and was dried under vacuum.

XRD data were collected on a PANalytical powder diffractometer using Cu Kα radiation. NiAu samples for XRD analysis were obtained by drying the ethanol-washed black powder product at 80 °C for 10 min, whereas catalyst samples were collected after specific pretreatment and reaction testing, unless otherwise indicated. TEM images were recorded on a Hitachi HD2000 scanning transmission electron microscope (STEM) system with an EDX attachment. NiAu samples for TEM experiments were the colloids redispersed in toluene. UV−visible spectra were obtained on a Varian Cary 5000 UV−vis−NIR spectrophotometer with a resolution of 2 nm. The NiAu samples reported in Figure 4 were the colloids redispersed in toluene, whereas the Ni samples for UV−vis experiments in Figure S2 were the original colloids since the small Ni clusters could not be isolated. TG/DTG experiments were conducted on a TGA 2950 instrument using a heating rate of 10 °C/min under air or N_2 atmosphere. FTIR spectroscopy was carried out in a diffuse reflectance cell (cell volume about 6 cm^3) in a Nicolet Nexus 670 FTIR spectrometer using a MCT/A detector with a spectral resolution of 4 cm^{-1}.

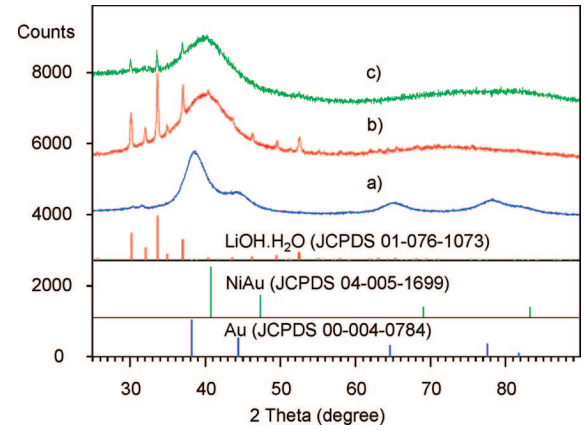

Figure 1. XRD patterns of NiAu samples aged at 120 °C: (a) sample prepared without the addition of trioctylphosphine and with the use of ethanol to wash the product; (b) sample prepared without the addition of trioctylphosphine and with the use of acetone to wash the product; (c) sample prepared with the addition of trioctylphosphine and washed by ethanol once. The standard data of $LiOH \cdot H_2O$ (JCPDS 01-076-1073), Au (JCPDS 00-004-0784), and NiAu alloy (JCPDS 04-005-1699) are listed for reference.

Catalytic CO oxidation was studied on an Altamira AMI 200 microreactor. Fifty milligrams of as-prepared $NiAu/SiO_2$ (2 wt % Au) was packed into a standard U-type quartz tube (4 mm i.d.), pretreated at 300−720 °C in H_2/He flow (H_2, 11 vol %) for 1 h, and then at 300−600 °C in O_2−He flow (O_2, 8 vol %) for 1 h. The catalyst was cooled down to room temperature, and the gas stream was switched to 1% CO (balance air) at a rate of 37 cm^3/min. A portion of the product stream was extracted periodically with an automatic sample valve and analyzed by a dual-column GC with a thermal conductivity detector.

3. Results and Discussion

3.1. Influence of Synthesis Details on the Formation of NiAu NPs. In our typical synthesis, Ni and Au precursors were coreduced by butyllithium in the presence of oleylamine at 40−50 °C, and the reaction mixture was aged at 120−260 °C and then cooled down to room temperature. Thereafter, trioctylphosphine was injected to protect the colloidal NPs, and ethanol was used to wash the product. Control experiments described below indicate that both the addition of trioctylphosphine and the choice of ethanol to wash the product are essential for obtaining clean NiAu NPs, and that the aging temperature also matters.

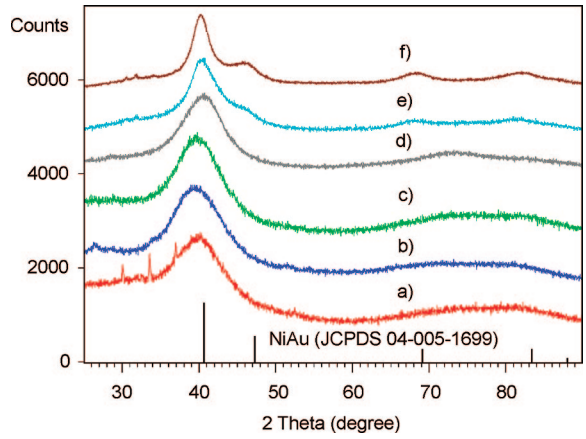

Figure 2. XRD patterns of NiAu alloy NPs aged at various temperatures: (a) 120 °C; (b) 150 °C; (c) 180 °C; (d) 210 °C; (e) 245 °C; (f) 260 °C. The standard data of NiAu alloy (JCPDS 04-005-1699) are listed for reference.

Figure 1 compares the XRD patterns of samples (aged at 120 °C) subject to different stabilization and solvent-washing conditions. The sample prepared without the addition of trioctylphosphine but with the use of ethanol to wash the product shows typical broad gold peaks at $2\theta = 38$, 44, 65, 78, and 82° (Figure 1a), indicating the dissolution of Ni component into ethanol without the proper protection of trioctylphosphine. To mitigate the leaching of Ni, we then attempted to use acetone instead of ethanol to wash the product, again without the addition of trioctylphosphine. This time, NiAu alloys are retained, as judged by the XRD profile showing the characteristic NiAu {111} peak around $2\theta = 40.7°$ (Figure 1b). However, the product washed by acetone contains significant amounts of $LiOH \cdot H_2O$ impurity, a byproduct formed by the reaction between C_4H_9Li and H_2O (Figure 1b). Relatively pure NiAu NPs can only be obtained using both trioctylphosphine as the protecting agent and ethanol to wash the product. In that case, most of residual $LiOH \cdot H_2O$ can be removed by a single ethanol washing (Figure 1c). Although $LiOH \cdot H_2O$ can be completely removed by a second ethanol washing, Ni is also partially dissolved into ethanol due to the high reactivity of the small NiAu NPs aged at 120 °C (data not shown). We will show in Figure 2 that all residual $LiOH \cdot H_2O$ coexistent with bigger NiAu NPs aged at higher temperatures can be washed away by repeated ethanol washing without suffering from the dissolution of Ni. Presumably this is because the surface free energy of larger NiAu NPs is lower, resulting in less reactive surface atoms, and because the bulky trioctylphosphine can more efficiently protect larger NiAu NPs.

The effect of different aging temperatures on the formation of NiAu NPs was studied by XRD and TEM. In principle, it is obvious to see whether the sample is NiAu alloy or a physical mixture of Ni and Au because the {111} diffractions of fcc NiAu ($2\theta = 40.7°$), Au ($2\theta = 38.2°$), and Ni ($2\theta = 44.5°$) are well separated. As shown in Figure 2, the XRD patterns of the sample aged at relatively low temperatures are broad, and high index diffractions are not resolved due to the dominance of small particles. More crystalline samples are formed when increasing the aging temperature above 245 °C, as indicated by the appearance of high index diffractions (traces e and f in Figure 2). Moreover, high-temperature aging in solution leads to the formation of more uniform NiAu alloy NPs, as indicated by the good match between the {111} diffraction of the samples aged above 210 °C and the {111} diffraction of NiAu in the database. In any case, XRD peaks ascribed to metallic Ni and

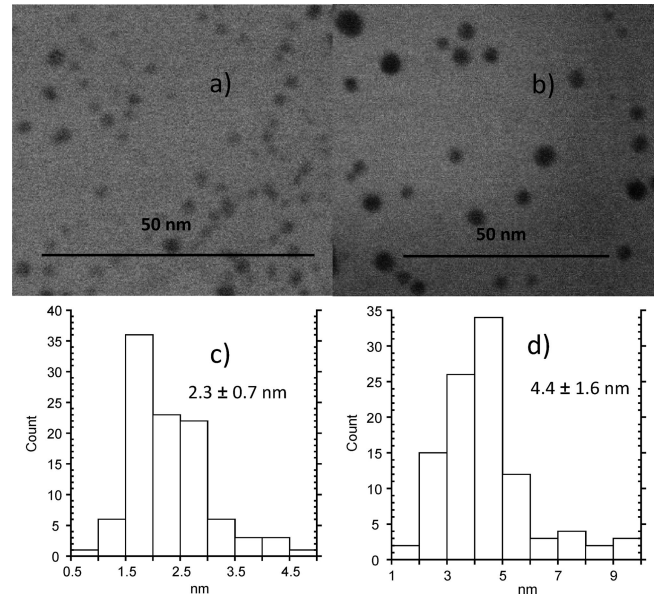

Figure 3. TEM images and particle size distributions of NiAu alloy NPs: (a) TEM image of NiAu sample aged at 120 °C; (b) TEM image of NiAu sample aged at 210 °C; (c) size distribution of NiAu NPs aged at 120 °C; (d) size distribution of NiAu NPs aged at 210 °C.

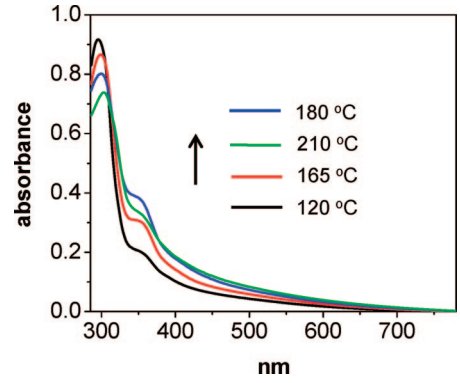

Figure 4. UV−vis spectra of NiAu samples aged at different temperatures.

Au are not observed with any aging temperature, and the composition of our samples is estimated from the position of {111} diffraction of NiAu aged at 260 °C as $Ni_{45}Au_{55}$. The formation of slightly Au-rich NiAu samples is probably due to some loss of Ni with ethanol washing or incomplete reduction of the Ni precursor. TEM images and particle size distribution of NiAu NPs aged at two different temperatures are shown in Figure 3. The NPs aged at 120 °C exhibit a mean size of 2.3 nm with a mainly spherical shape (Figure 3a, c). For comparison, the NPs aged at 210 °C have a mean size of 4.4 nm (Figure 3b, d).

Above, we have elaborated on the effects of synthesis details (protecting agent, washing solvent, and aging temperature) on the formation of products and have used XRD to demonstrate that the bimetallic NiAu NPs synthesized at 120−260 °C are indeed NiAu alloy NPs rather than physical mixtures of Ni and Au. To further confirm the formation of NiAu alloy NPs unequivocally, we have characterized an NiAu alloy sample aged at 210 °C by HRTEM, EDX, UV−vis, and XPS in great detail and have reported these results elsewhere.[26] Figure S1 in the Supporting Information, reproduced from our communication,[26] shows an HRTEM image of one NiAu alloy particle aged at 210 °C. The *d*-spacing of the NiAu {111} lattice is determined to be 2.2 Å, consistent with the XRD data.

3.2. Study of Synthesis Mechanism. NiAu alloys are difficult to obtain because Au ions are much easier to be reduced than Ni ions, and bulk Ni and Au are immiscible. However, here we obtained NiAu alloy NPs rather than the more stable Ni@Au core−shell structures. To explain our unique finding, we first describe the visual observations that may provide clues to the synthesis mechanism. In our synthesis, the precursor mixture was mildly heated (around 40−50 °C) to dissolve the reagents completely, and dark brown colloids were formed immediately after injecting this warm precursor solution to the butyllithium solution. In contrast, Au NPs synthesized under our experimental conditions are reddish, and Ni NPs are dark green. Thus, the immediate appearance of the dark brown color of the NiAu colloids suggests coreduction rather than sequential reduction of the Ni and Au precursors where sequential color changes are expected. This coreduction with butyllithium was also observed in the synthesis of AuPt alloy NPs.[12]

To demonstrate the advantage of using butyllithium in the facile reduction of Ni cations, we compared this butyllithium reduction method with a thermal decomposition method.[34] In the butyllithium reduction of $Ni(acac)_2$, dark green Ni colloids can be formed even at room temperature. Reducing $Ni(acac)_2$ at 120−210 °C leads to dark green Ni colloids as well. These Ni clusters cannot be isolated because they are lost during the washing and centrifugation process, implying that these Ni clusters are very small and highly reactive. For comparison, we attempted to synthesize Ni NPs using a modified method by thermal decomposition of Ni(II)−trioctylphosphine complex.[34] $Ni(acac)_2$, oleylamine, and trioctylphosphine were the starting materials, and dioctyl ether was the solvent, but no butyllithium was added. Following the decomposition at 120 and 165 °C, the solution still remains a clear blue solution. Dark green Ni colloids are formed by increasing the decomposition temperature to 210 °C. Therefore, the butyllithium reduction is much more effective than the decomposition of Ni(II)−trioctylphosphine complex in reducing Ni species.

More evidence for the coreduction mechanism can be gleaned from characterizing the products aged at different temperatures. The absence of individual Au or Ni diffractions in the XRD patterns of NiAu samples aged at 120−260 °C may support the coreduction mechanism (Figure 2). The UV−vis data of NiAu samples aged at different temperatures also prove the formation of bimetallic alloy (Figure 4). It is known that Au NPs larger than 2 nm exhibit an SPR band around 530 nm. Since our NiAu NPs are all larger than 2 nm, the absence of the Au SPR band at 530 nm excludes the presence of monometallic Au NPs or Ni@Au core−shell structures. On the other hand, an absorption feature centered at 365 nm is observed with NiAu colloids (Figure 4) and Ni NPs (Figure S2a) prepared by butyllithium reduction but is not observed with Ni NPs prepared by decomposition of Ni(II)−trioctylphosphine at 210 °C (Figure S2b). Since the former preparation method involves the use of butyllithium, and the latter does not, the 365 nm band may originate from the surface Ni(0)−alkyl charge transfer. Therefore, it appears that metallic Ni atoms are present on the surfaces of NiAu NPs aged at 120−260 °C.

From the above-mentioned mechanistic study, a picture of the formation of NiAu alloys can be obtained. The first point is that the fast coreduction of the Ni and Au precursors by butyllithium guarantees the formation of bimetallic NPs. The second point is that the small size of bimetallic NPs nanoclusters facilitates the mass diffusion of Ni and Au to form uniform NiAu alloy NPs. For comparison, the mass diffusion from solid to solid in the bulk is the rate-limiting step in the solid-state method, and hence the formation of NiAu alloy takes place at 750 °C.[12] The third point is that the stabilization by trioctylphosphine traps the Ni atoms on the particle surfaces and prevents the Ni atoms from migration into the inner part of NPs to form thermodynamically stable Ni@NiAu or Ni@Au core−shell structures. As a result, uniform solid-solution NiAu alloy NPs are successfully synthesized through the combination of these three features.

3.3. Catalytic CO Oxidation on Supported Catalysts. Gold catalysis has been actively studied recently because it has many applications in environmental catalysis, energy catalysis, and chemical synthesis.[28−33] The majority of gold catalysts are prepared by loading a gold precursor or gold colloids onto a support (e.g., TiO_2) by deposition−precipitation or other methods. Some gold-containing alloy NPs have been used to prepare supported alloy catalysts, such as PdAu/zeolite-Y,[35] $PdAu/TiO_2$,[36] $PdAu/Fe_2O_3$,[37] $PdAu/TiO_2-SiO_2$,[38] $PdAu/CeO_2$,[39] $PdAu/SiO_2$,[40] PdAu/C,[41] $AuRu/Fe_2O_3$,[42] $AuNi/Fe_2O_3$,[42] $AgAu/SiO_2$,[43,44] $AuCu/SiO_2$,[45] and $AuAg/SiO_2$.[46] Nevertheless, the focus has always been placed on bimetallic alloys rather than on the use of alloys as the precursor to design advanced structured catalysts. In the current work we supported 210 °C-aged NiAu alloy NPs on SiO_2 and obtained heterostructured $Au-NiO/SiO_2$ catalysts via proper pretreatment. We then tested the resulting catalysts in CO oxidation as a probe reaction.

3.3.1. Pretreating NiAu/SiO$_2$ Solely in O$_2$. Supported catalysts are commonly pretreated at elevated temperatures to remove the moisture and volatile impurities prior to reaction testing. We previously found that the pretreatment of $Au/M_xO_y/TiO_2$,[47] $Au/MnO_x/C$,[48] $SiO_2/Au/TiO_2$,[49] and Au/M−P−O[50] catalysts under O_2 at elevated temperatures is sufficient to obtain active catalysts. Therefore, we also attempted to pretreat $NiAu/SiO_2$ in O_2 at 300 or 600 °C in initial catalytic testing. As shown in the top panel of Figure 5, the 300 °C-pretreated sample is not particularly active (T_{50} = 199 °C, trace a), whereas the 600 °C-pretreated catalyst is much more active (T_{50} = 29 °C, trace b), although there is an anomalous dip in its conversion curve.

According to the XRD data in Figure S3, the catalyst pretreated at either 300 or 600 °C contains both SiO_2 and metallic gold, whereas neither NiAu nor NiO is detected. The NiO species formed by oxidation of the Ni component in O_2 is presumably amorphous and thus cannot be detected by XRD. This is understandable, because the amount of NiO on support surface is calculated as 0.8 wt %, considering the gold loading (2 wt %) and the mole ratio of gold and nickel (1:1). The gold peaks are sharper as the pretreatment temperature increases, indicating the sintering of gold nanoparticles, and the mean gold particle sizes of the samples are determined by TEM as 3.3 and 7.9 nm, respectively (Figure S4). The higher activity of the 600 °C-pretreated sample may be due to the more complete removal of organic residuals on catalyst surfaces (trace a in Figure 6)[51−60] as well as the enhanced development of NiO and better phase separation of Au and NiO components at elevated temperatures. We speculate that the former factor may be less important because according to TG/DTG data, it is sufficient to remove most of the organics at 300 °C (trace a in Figure 6).

3.3.2. Pretreating NiAu/SiO$_2$ in H$_2$ and Then in O$_2$. To find the optimal pretreatment conditions, we then tried to pretreat the catalyst in H_2 at high temperatures followed by O_2 treatment (the middle panel of Figure 5). The catalyst pretreated in H_2 at 300 °C and then in O_2 at 300 °C is not particularly active (T_{50} = 200 °C, trace c), similar to the one solely pretreated in O_2 at 300 °C (T_{50} = 199 °C, trace a). Higher CO conversion at low

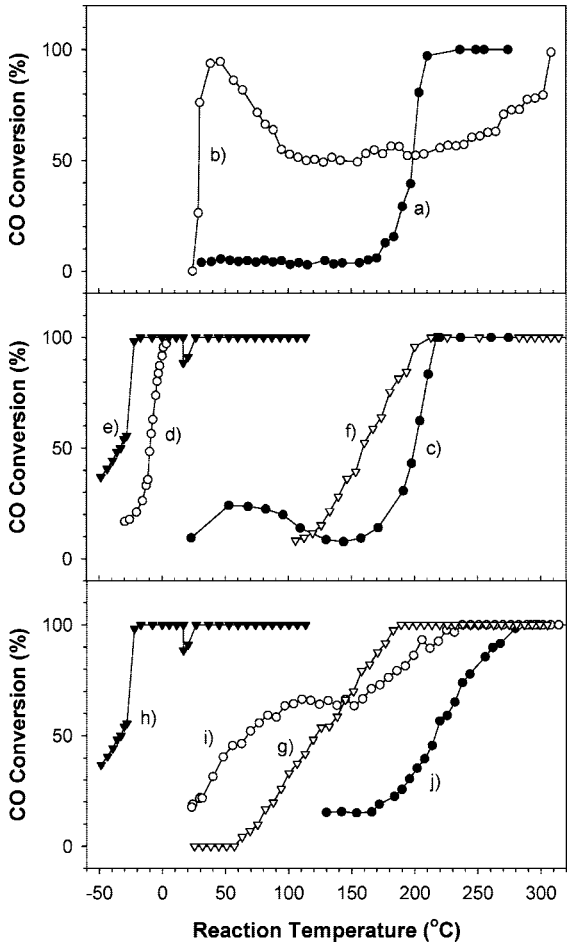

Figure 5. Top and middle panels: CO oxidation on SiO_2-supported NiAu following different pretreatments: (a) 300 °C in O_2; (b) 600 °C in O_2; (c) 300 °C in H_2, 300 °C in O_2; (d) 600 °C in H_2, 300 °C in O_2; (e) 720 °C in H_2, 300 °C in O_2; (f) 600 °C in H_2. Bottom panel: CO oxidation on Ni_3Au/SiO_2-derived catalyst (g); $NiAu/SiO_2$-derived catalyst (h); $NiAu_3/SiO_2$-derived catalyst (i); Au/SiO_2 (j) pretreated at 720 °C in H_2 and 300 °C in O_2.

temperatures is obtained if the catalyst is pretreated in H_2 at 600 or 720 °C and O_2 at 300 °C ($T_{50} = -10$ and -33 °C, traces d and e, respectively). XRD data acquired after the pretreatment show only the presence of metallic gold and no indication of metallic Ni (Figure S5). The presence of metallic gold and amorphous NiO has been previously confirmed by EXAFS.[26] TEM data indicate that the catalyst pretreated in H_2 at 300, 600, or 720 °C and in O_2−He at 300 °C has mean metallic particle size of roughly 4 nm (Figure S6).

To explain why the catalytic activity is improved by sequentially pretreating the catalyst in H_2 at 600 or 720 °C and in O_2 at 300 °C, we first discuss why the pretreatment of the catalyst solely in H_2 at 600 °C is not sufficient to achieve high activity ($T_{50} = 159$ °C, trace f). First, NiAu NPs cannot be oxidized to the active Au−NiO under such reducing conditions. Second, TG/DTG measurement of the catalyst under inert atmosphere (N_2) shows that the weight loss of organic moieties (trace b in Figure 6) is obviously less than the weight loss under air (trace a in Figure 6). In addition, FT-IR experiments using CO as a probe did not detect CO adsorption on the sample solely pretreated in H_2 at 720 °C (data not shown), indicating that high-temperature H_2 treatment does not eliminate all of the organic moieties on the surface of NPs and the catalytic metal surfaces may still be covered by surfactant-derived species. In the literature, the activation of organic moiety-containing metal NPs

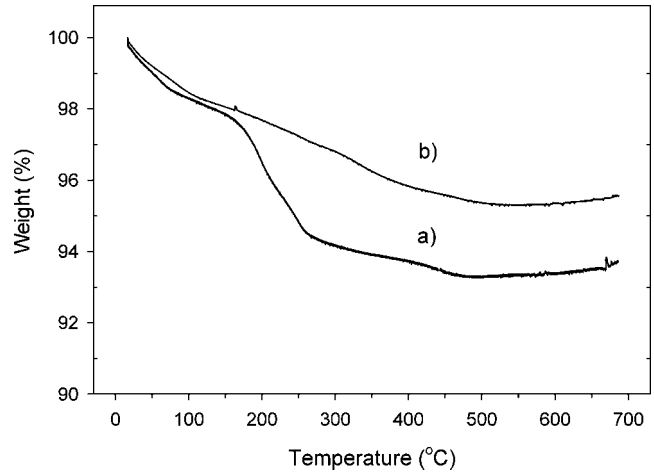

Figure 6. TG curves of $NiAu/SiO_2$ under air (trace a) or N_2 (trace b) ambient.

in nonoxidative gases could lead to the formation of carbon deposit on metal surfaces.[61]

A model is therefore proposed to explain the roles of sequentially pretreating the catalyst in H_2 at 600 or 720 °C and in O_2 at 300 °C. High-temperature H_2 pretreatment facilitates the dealloying of the NiAu NPs to form Au-rich@Ni-rich core−shell structures.[26] The subsequent O_2 treatment removes more residual organic moieties, oxidizes the Ni component, and facilitates proper phase separation of Au NPs and the NiO component. We have performed a thorough characterization of SiO_2-supported Au−NiO catalyst by XRD, EXAFS, TEM, and single-particle quantitative EDX, and demonstrated that the catalyst after the optimal pretreatment is actually $Au-NiO/SiO_2$, with the Au distributed on or near the amorphous NiO.[26] In addition, a survey FT-IR experiment using CO adsorption as a probe indicates that the majority of Ni is in its cationic state (peak position at 2174 cm^{-1}) and Au is in its metallic state (peak position at 2111 cm^{-1}) after treating $NiAu/SiO_2$ in H_2 at 720 °C and O_2 at 300 °C. The presence of amorphous NiO in the proximity of gold nanoparticles on SiO_2 may not only stabilize gold nanoparticles but also promote the activity.

3.3.3. Effect of Catalyst Composition. Finally, the influence of Ni/Au ratio in the pretreated catalyst on catalytic performance was studied. As shown in the bottom panel of Figure 5, the catalytic activity follows a trend in which the highest catalytic activity is maximum for the catalyst with Ni/Au = 1. Higher or lower Ni/Au ratios, including pure Au, result in decreased catalytic activity. The drastic difference in activity is already very clear in view of the well-separated conversion curves in the bottom panel of Figure 5. Also because of the drastic difference in activity, it is not convenient to compare the specific rates of four catalysts at one reaction temperature. Table S1 lists the specific rates achieved by these catalysts at different temperatures. In general, the higher the specific rate at a lower reaction temperature, the higher the catalytic activity. From Table S1, it is still clear that the catalyst with Ni/Au = 1 is the most active one.

The catalysts collected after suitable pretreatment and catalytic reaction were characterized. The only features observable in the XRD data are due to metallic gold, and the variation in the width of the Au diffraction features indicate that the gold particle sizes increase with increasing Au concentration (Figure 7). The mean gold particle sizes of these four samples are determined by dark-field TEM to be 3.7, 3.6, 7.8, and 36.5 nm, with increasing Au content (Figures 8 and S7), consistent with the

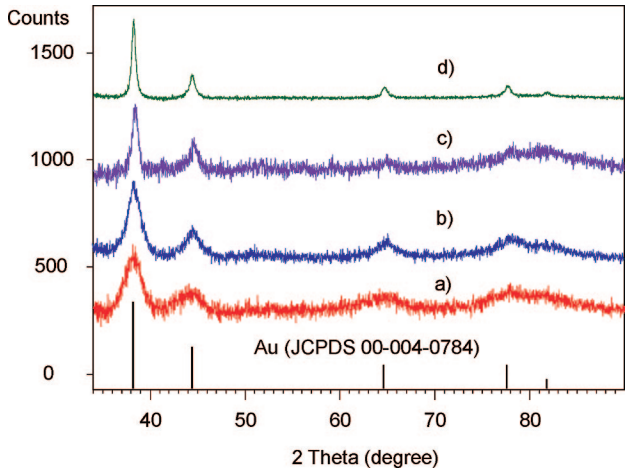

Figure 7. XRD patterns of samples collected after 720 °C pretreatment in H_2, 300 °C pretreatment in O_2, and reaction testing: (a) Ni_3Au/SiO_2; (b) $NiAu/SiO_2$; (c) $NiAu_3/SiO_2$; (d) Au/SiO_2. The background has been subtracted to obtain clear comparison between these catalysts. The standard data Au (JCPDS 00-004-0784) are listed for reference.

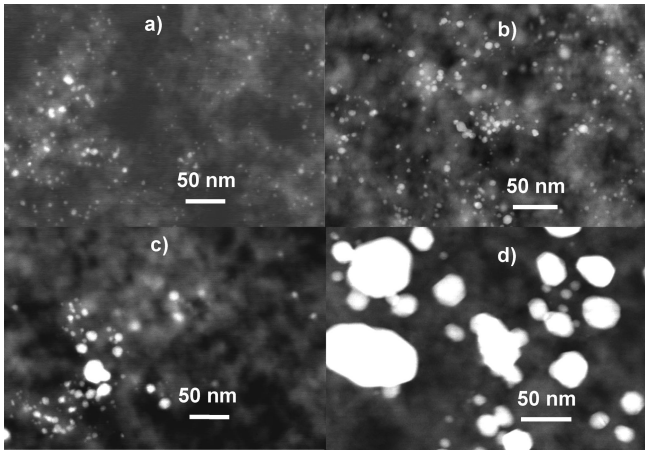

Figure 8. Dark-field TEM images of samples collected after 720 °C pretreatment in H_2, 300 °C pretreatment in O_2, and reaction testing: (a) Ni_3Au/SiO_2-derived catalyst; (b) $NiAu/SiO_2$-derived catalyst; (c) $NiAu_3/SiO_2$-derived catalyst; (d) Au/SiO_2.

trend seen in XRD data. It is clear that the thermal stability of gold nanoparticles is related to the composition of the catalysts. The low activity of Au/SiO_2 is due to the growth of large gold nanoparticles that sinter easily on SiO_2. The Ni_3Au/SiO_2-derived catalyst is less active than the $NiAu/SiO_2$-derived catalyst, probably because the small gold nanoparticles are covered by too much NiO.

Compared with Au/SiO_2 prepared by the dispersion of Au colloids on SiO_2, the advantage of our $Au-NiO/SiO_2$ is that the gold particle size can be controlled after high-temperature treatments. Note that the activity of Au/SiO_2 in CO oxidation is low in most previous reports,[51,53,55,62−64] and high CO conversion below 0 °C can only be achieved on Au/SiO_2 prepared using $Au(en)_2Cl_3$ as the precursor.[65,66] Using $Au(en)_2Cl_3$ as the precursor, Au/SiO_2 catalysts have predominately small gold nanoparticles and high thermal stability.[65,66] Although the optimal pretreatment conditions are not the same in different studies, the catalytic activity of the current $Au-NiO/SiO_2$ (2.0 wt % Au, $T_{50} = -33$ °C) is still higher than or at least comparable to that of Au/SiO_2 (2.5 wt % Au, $T_{50} = -8$ °C) and $Au/NiO/SiO_2$ (2.0 wt % Au, $T_{50} = -15$ °C) prepared using $Au(en)_2Cl_3$ as the precursor.[66] To compare these catalysts another way, the CO conversions on these catalysts at −30 °C are 54, 27, and 21%, respectively, and the specific rates are calculated as 0.49, 0.20, and 0.19 $mol \cdot g_{Au}^{-1} \cdot h^{-1}$, respectively (Table S1).

3.4. Discussion in the Context of Catalyst Design. Traditionally, gold catalysts (e.g., Au/TiO_2) are prepared by loading gold on supports via deposition−precipitation, impregnation, and other methods.[28−32] The resulting catalysts have simple metal−support interfaces, limited catalytic functionalities, and often poor thermal stability. Several strategies for the rational design of advanced gold catalysts have been generalized.[67] These strategies include premodification of the support by an oxide modifier before loading gold (e.g., $Au/CoO_x/SiO_2$,[68,69] $Au/TiO_2/SiO_2$,[70,71] $Au/MnO_x/Al_2O_3$,[72] $Au/TiO_2/Al_2O_3$,[73] $Au/M_xO_y/TiO_2$,[47,74] and $Au/MnO_x/C$[48]), postmodification of a supported gold catalyst by an oxide modifier (e.g., $FeO_x/Au/TiO_2$,[75] $SiO_2/Au/TiO_2$,[49,76] and $MnO_x/Au/SiO_2$[77]), and loading preformed metal−metal oxide composites onto a solid support (e.g., $Au-Fe_3O_4/SiO_2$[78]). The resulting catalysts may have metal−support, metal−modifier, and modifier−support interfaces, and the catalytic performance may be tuned by such modification. For instance, we treated $Au(en)_2Cl_3$-derived Au/SiO_2 in $KMnO_4$ solution and calcined the sample at elevated temperatures to form additional $Au-MnO_x$ and MnO_x-SiO_2 interfaces, and the resulting $MnO_x/Au/SiO_2$ catalyst showed high activity in low-temperature CO oxidation.[77] We also dispersed preformed dumbbell-like $Au-Fe_3O_4$ colloids[79] onto SiO_2 and other supports, resulting in the formation of complex interfacial structures more resistant to catalyst sintering.[78] Although these works enriched the literature database on advanced gold catalysts, the development of new methodologies for the design of advanced gold catalysts is still desirable.

The present work furnishes yet another design strategy by introducing an alloyed active metal (Au) and a precursor (Ni) of an oxide modifier (NiO) simultaneously onto a solid support (SiO_2). The synthesis of 1:1 NiAu alloy NPs guarantees the homogeneous mixing of Ni and Au on SiO_2 surfaces. After phase separation and oxidation (i.e., proper H_2 and O_2 pretreatments), the localized presence of amorphous NiO in the final catalyst may stabilize gold nanoparticles since we found that, in contrast, gold nanoparticles on neat SiO_2 support sinter much more dramatically at elevated temperatures. The formation of Au/NiO heteroaggregate nanostructure from a single-particle precursor maximizes Au−NiO interactions while minimizing the quantity of Ni required to enhance activity and thermal stability. Our previous TEM and single-particle EDX experiments have provided detailed evidence for the enrichment of Ni element near gold nanoparticles.[26]

Although the in situ transformation of bimetallic alloys to metal−metal oxide composite structures is not often reported, it has general occurrence. For example, Baiker and co-workers used amorphous metal glasses (e.g., Pd−Zr alloy) as the precursor for making metal/metal oxide catalysts (e.g., Pd/ZrO_2),[80−82] Yang and co-workers reported the synthesis of FePt nanoparticles and their transformation to $Pt@Fe_2O_3$ nanoparticles,[9] Xie and co-workers synthesized $Au@SnO_2$ catalysts via the oxidation of AuSn nanoparticles,[83] and Schaak and co-workers synthesized a Bi_2O_3/Pd nanocomposite via the oxidation of Bi_2Pd nanocubes.[84] Nevertheless, the catalytic activity was often not reported or very low, sometimes due to the encapsulation of metal nanoparticles in the oxide shells and the difficulty in obtaining small metal particles of catalysis relevance. The gold nanoparticles in our current work are very small, and they are active for low-temperature CO oxidation under careful preparation and pretreatment conditions. It is expected that this in situ

transformation strategy may prompt the development of new advanced catalysts with unusual chemical and structural properties.

4. Conclusions

In this work, NiAu alloy NPs were prepared by a facile low-temperature solution-phase method. In the controlled synthesis, Au^{3+} and Ni^{2+} were coreduced by butyllithium. The resulting dark brown colloids were aged at 120−260 °C, cooled down to room temperature, protected by adding trioctylphosphine, and washed by ethanol. The following were found: (1) butyllithium plays an important role in the easily achieved reduction of both Au^{3+} and Ni^{2+}; (2) aging temperature influences the size of NiAu alloy NPs; (3) trioctylphosphine can protect the NiAu alloy NPs so as to avoid the leaching of the Ni component in ethanol; (4) ethanol solvent is better than acetone to remove the unwanted $LiOH \cdot H_2O$ byproduct. Overall, the successful synthesis of the thermodynamically metastable NiAu alloy phase at relatively low temperatures is due to the rapid coreduction by butyllithium reduction, facile intermixing of Ni and Au atoms inside small NPs, and stabilization by the protecting agent.

NiAu alloy NPs were used as the precursor to SiO_2-supported catalysts. It was found that the pretreatment prior to reaction testing plays an important role in determining the activity in CO oxidation due to competing processes of removal of organics, oxidation of Ni, and growth of Au particles. Pretreating the catalyst under optimal conditions, i.e., in H_2 at 600 or 720 °C followed by treating in O_2 at 300 °C, results in an Au−NiO/SiO_2 catalyst that is highly active in CO oxidation. For comparison, solely pretreating the NiAu/SiO_2 sample in H_2 does not lead to a reasonably active catalyst. The Ni/Au ratio in the precursor NPs is also important for determining the final structure and catalytic activity. The most active Au−NiO/SiO_2 catalyst was obtained by keeping the Ni/Au ratio at 1:1.

This work furnishes a new strategy for designing multiple-component gold catalysts by using bimetallic alloys as the precursors. In more general terms, the commonly used supported bimetallic catalysts often have big particle sizes and irregular shapes, hence the current NiAu/SiO_2 with controllable small alloy particle sizes may provide valuable information for the design of novel bimetallic nanocatalysts. Although here we have chosen the synthesis of NiAu alloy NPs as an example and CO oxidation as a probe reaction, further work may be conducted by varying the elemental composition of the alloy NPs and supported catalysts, as well as by demonstrating their wider applications in other suitable reactions.

Acknowledgment. Research was sponsored by the Division of Chemical Sciences, Geosciences, and Biosciences, Office of Basic Energy Sciences, U.S. Department of Energy, under contract DE-AC05-00OR22725 with Oak Ridge National Laboratory, managed and operated by UT-Battelle, LLC. A portion of this research was carried out at Oak Ridge National Laboratory's Center for Nanophase Materials Sciences and was sponsored by the Scientific User Facilities Division, Office of Basic Energy Sciences, U.S. Department of Energy. S.Z., Z.M., and H.Y. are sponsored by an appointment to the ORNL Research Associates Program administered jointly by Oak Ridge Associated Universities and Oak Ridge National Laboratory.

Supporting Information Available: Figures S1−S7 and Table S1. This information is available free of charge via the Internet at http://pubs.acs.org.

References and Notes

(1) Wang, Y.; Toshima, N. *J. Phys. Chem. B* **1997**, *101*, 5301.
(2) Son, S. U.; Jang, Y.; Park, J.; Na, H. B.; Park, H. M.; Yun, H. J.; Lee, J.; Hyeon, T. *J. Am. Chem. Soc.* **2004**, *126*, 5026.
(3) Lee, W. R.; Kim, M. G.; Choi, J. R.; Park, J. I.; Ko, S. J.; Oh, S. J.; Cheon, J. *J. Am. Chem. Soc.* **2005**, *127*, 16090.
(4) Zhou, S. H.; Varughese, B.; Eichhorn, B.; Jackson, G.; McIlwrath, K. *Angew. Chem., Int. Ed. Engl.* **2005**, *44*, 4539.
(5) Chen, D.; Li, J. J.; Shi, C. S.; Du, X. W.; Zhao, N. Q.; Sheng, J.; Liu, S. *Chem. Mater.* **2007**, *19*, 3399.
(6) Alayoglu, S.; Nilekar, A. U.; Mavrikakis, M.; Eichhorn, B. *Nat. Mater.* **2008**, *7*, 333.
(7) Tao, F.; Grass, M. E.; Zhang, Y. W.; Butcher, D. R.; Renzas, J. R.; Liu, Z.; Chung, J. Y.; Mun, B. S.; Salmeron, M.; Somorjai, G. A. *Science* **2008**, *322*, 932.
(8) Gu, H. W.; Yang, Z. M.; Gao, J. H.; Chang, C. K.; Xu, B. *J. Am. Chem. Soc.* **2005**, *127*, 34.
(9) Teng, X. W.; Yang, H. *J. Am. Chem. Soc.* **2003**, *125*, 14559.
(10) Sra, A. K.; Schaak, R. E. *J. Am. Chem. Soc.* **2004**, *126*, 6667.
(11) Scott, R. W. J.; Sivadinarayana, C.; Wilson, O. M.; Yan, Z.; Goodman, D. W.; Crooks, R. M. *J. Am. Chem. Soc.* **2005**, *127*, 1380.
(12) Zhou, S. H.; Jackson, G. S.; Eichhorn, B. *Adv. Funct. Mater.* **2007**, *17*, 3099.
(13) Liu, J.-H.; Wang, A.-Q.; Chi, Y.-S.; Lin, H.-P.; Mou, C.-Y. *J. Phys. Chem. B* **2005**, *109*, 40.
(14) Edwards, J. K.; Hutchings, G. J. *Angew. Chem., Int. Ed. Engl.* **2008**, *47*, 9192.
(15) Ferrando, R.; Jellinek, J.; Johnston, R. L. *Chem. Rev.* **2008**, *108*, 845.
(16) Molenbroek, A. M.; Norskov, J. K.; Clausen, B. S. *J. Phys. Chem. B* **2001**, *105*, 5450.
(17) Triantafyllopoulos, N. C.; Neophytides, S. G. *J. Catal.* **2006**, *239*, 187.
(18) Chin, Y. H.; King, D. L.; Roh, H. S.; Wang, Y.; Heald, S. M. *J. Catal.* **2006**, *244*, 153.
(19) Yuan, G.; Louis, C.; Delannoy, L.; Keane, M. A. *J. Catal.* **2007**, *247*, 256.
(20) Besenbacher, F.; Chorkendorff, I.; Clausen, B. S.; Hammer, B.; Molenbroek, A. M.; Nørskov, J. K.; Stensgaard, I. *Science* **1998**, *279*, 1913.
(21) Wang, J. H.; Lu, X. G.; Sundman, B.; Su, X. P. *Calphad* **2005**, *29*, 263.
(22) Okamoto, H.; Massalski, T. B. In *American Society for Metals*; Materials Park, 1991; p 16.
(23) Lu, D. L.; Domen, K.; Tanaka, K. *Langmuir* **2002**, *18*, 3226.
(24) Schaak, R. E.; Sra, A. K.; Leonard, B. M.; Cable, R. E.; Bauer, J. C.; Han, Y. F.; Means, J.; Teizer, W.; Vasquez, Y.; Funck, E. S. *J. Am. Chem. Soc.* **2005**, *127*, 3506.
(25) Leonard, B. M.; Bhuvanesh, N. S. P.; Schaak, R. E. *J. Am. Chem. Soc.* **2005**, *127*, 7326.
(26) Zhou, S. H.; Yin, H. F.; Schwartz, V.; Wu, Z. L.; Mullins, D. R.; Eichhorn, B.; Overbury, S. H.; Dai, S. *Chem. Phys. Chem.* **2008**, *9*, 2475.
(27) Vasquez, Y.; Luo, Z. P.; Schaak, R. E. *J. Am. Chem. Soc.* **2008**, *130*, 11866.
(28) Haruta, M.; Daté, M. *Appl. Catal., A* **2001**, *222*, 427.
(29) Choudhary, T. V.; Goodman, D. W. *Top. Catal.* **2002**, *21*, 25.
(30) Hashmi, A. S. K.; Hutchings, G. J. *Angew. Chem., Int. Ed. Engl.* **2006**, *45*, 7896.
(31) Bond, G. C.; Louis, C.; Thompson, D. T. *Catalysis by Gold*; Imperial College Press: London, 2006.
(32) Kung, M. C.; Davis, R. J.; Kung, H. H. *J. Phys. Chem. C* **2007**, *111*, 11767.
(33) Corti, C. W.; Holliday, R. J.; Thompson, D. T. *Top. Catal.* **2007**, *44*, 331.
(34) Park, J.; Kang, E.; Son, S. U.; Park, H. M.; Lee, M. K.; Kim, J.; Kim, K. W.; Noh, H. J.; Park, J. H.; Bae, C. J.; Park, J. G.; Hyeon, T. *Adv. Mater.* **2005**, *17*, 429.
(35) Riahi, G.; Guillemot, D.; Polisset-Thfoin, M.; Khodadadi, A. A.; Fraissard, J. *Catal. Today* **2002**, *72*, 115.
(36) Edwards, J. K.; Solsona, B. E.; Landon, P.; Carley, A. F.; Herzing, A.; Kiely, C. J.; Hutchings, G. J. *J. Catal.* **2005**, *236*, 69.
(37) Edwards, J. K.; Solsona, B.; Landon, P.; Carley, A. F.; Herzing, A.; Watanabe, M.; Kiely, C. J.; Hutchings, G. J. *J. Mater. Chem.* **2005**, *15*, 4595.
(38) Zwijnenburg, A.; Saleh, M.; Makkee, M.; Moulijn, J. A. *Catal. Today* **2002**, *72*, 59.
(39) Kapoor, M. P.; Ichihashi, Y.; Nakamori, T.; Matsumura, Y. *J. Mol. Catal. A* **2004**, *213*, 251.
(40) Bonarowska, M.; Pielaszek, J.; Juszczyk, W.; Karpinski, Z. *J. Catal.* **2000**, *195*, 304.
(41) Bonarowska, M.; Pielaszek, J.; Semikolenov, V. A.; Karpinski, Z. *J. Catal.* **2002**, *209*, 528.
(42) Venugopal, A.; Aluha, J.; Scurrell, M. S. *Catal. Lett.* **2003**, *90*, 1.
(43) Wang, A. Q.; Chang, C. M.; Mou, C. Y. *J. Phys. Chem. B* **2005**, *109*, 18860.

(44) Wang, A. Q.; Hsieh, Y.-P.; Chen, Y.-F.; Mou, C.-Y. *J. Catal.* **2006**, *237*, 197.
(45) Liu, X. Y.; Wang, A. Q.; Wang, X. D.; Mou, C. Y.; Zhang, T. *Chem. Commun.* **2008**, 3187.
(46) Liu, X. Y.; Wang, A. Q.; Yang, X. F.; Zhang, T.; Mou, C. Y.; Su, D. S.; Li, J. *Chem. Mater.* **2009**, *21*, 410.
(47) Ma, Z.; Overbury, S. H.; Dai, S. *J. Mol. Catal. A* **2007**, *273*, 186.
(48) Ma, Z.; Liang, C. D.; Overbury, S. H.; Dai, S. *J. Catal.* **2007**, *252*, 119.
(49) Ma, Z.; Brown, S.; Howe, J. Y.; Overbury, S. H.; Dai, S. *J. Phys. Chem. C* **2008**, *112*, 9448.
(50) Ma, Z.; Yin, H. F.; Overbury, S. H.; Dai, S. *Catal. Lett.* **2008**, *126*, 20.
(51) Yuan, Y. Z.; Asakura, K.; Wan, H. L.; Tsai, K.; Iwasawa, Y. *Catal. Lett.* **1996**, *42*, 15.
(52) Choudhary, T. V.; Sivadinarayana, C.; Chusuei, C. C.; Datye, A. K.; Fackler, J. P.; Goodman, D. W. *J. Catal.* **2002**, *207*, 247.
(53) Martra, G.; Prati, L.; Manfredotti, C.; Biella, S.; Rossi, M.; Coluccia, S. *J. Phys. Chem. B* **2003**, *107*, 5453.
(54) Wu, S.-H.; Zheng, X.-C.; Wang, S.-R.; Han, D.-Z.; Huang, W.-P.; Zhang, S.-M. *Catal. Lett.* **2004**, *96*, 49.
(55) Chou, J.; Franklin, N. R.; Baeck, S.-H.; Jaramillo, T. F.; McFarland, E. W. *Catal. Lett.* **2004**, *95*, 107.
(56) Yan, Z.; Chinta, S.; Mohamed, A. A.; Fackler, J. P.; Goodman, D. W. *Catal. Lett.* **2006**, *111*, 15.
(57) Menard, L. D.; Xu, F. T.; Nuzzo, R. G.; Yang, J. C. *J. Catal.* **2006**, *243*, 64.
(58) Zheng, N. F.; Stucky, G. D. *J. Am. Chem. Soc.* **2006**, *128*, 14278.
(59) Chiang, C.-W.; Wang, A. Q.; Mou, C.-Y. *Catal. Today* **2006**, *117*, 220.
(60) Budroni, G.; Corma, A. *Angew. Chem., Int. Ed. Engl.* **2006**, *45*, 3328.
(61) Chaubey, G. S.; Barcena, C.; Poudyal, N.; Rong, C. B.; Gao, J. M.; Sun, S. H.; Liu, J. P. *J. Am. Chem. Soc.* **2007**, *129*, 7214.
(62) Overbury, S. H.; Ortiz-Soto, L.; Zhu, H. G.; Lee, B.; Amiridis, M. D.; Dai, S. *Catal. Lett.* **2004**, *95*, 99.
(63) Bore, M. T.; Pham, H. N.; Switzer, E. E.; Ward, T. L.; Fukuoka, A.; Datye, A. K. *J. Phys. Chem. B* **2005**, *109*, 2873.
(64) Delannoy, L.; El Hassan, N.; Musi, A.; Le To, N. N.; Krafft, J.-M.; Louis, C. *J. Phys. Chem. B* **2006**, *110*, 22471.
(65) Zhu, H. G.; Liang, C. D.; Yan, W. F.; Overbury, S. H.; Dai, S. *J. Phys. Chem. B* **2006**, *110*, 10842.
(66) Zhu, H. G.; Ma, Z.; Clark, J. C.; Pan, Z. W.; Overbury, S. H.; Dai, S. *Appl. Catal., A* **2007**, *326*, 89.
(67) Ma, Z.; Overbury, S. H.; Dai, S. In *Nanomaterials: Inorganic and Bioinorganic Perspectives*; Lukehart, C. M., Scott, R. A., Eds.; John Wiley & Sons: Chichester, 2009; article ID ia407.
(68) Dekkers, M. A. P.; Lippits, M. J.; Nieuwenhuys, B. E. *Catal. Today* **1999**, *54*, 381.
(69) Qian, K.; Huang, W. X.; Jiang, Z. Q.; Sun, H. X. *J. Catal.* **2007**, *248*, 137.
(70) Yan, W. F.; Chen, B.; Mahurin, S. M.; Hagaman, E. W.; Dai, S.; Overbury, S. H. *J. Phys. Chem. B* **2004**, *108*, 2793.
(71) Yan, W. F.; Mahurin, S. M.; Chen, B.; Overbury, S. H.; Dai, S. *J. Phys. Chem. B* **2005**, *109*, 15489.
(72) Grisel, R. J. H.; Nieuwenhuys, B. E. *Catal. Today* **2001**, *64*, 69.
(73) Yan, W. F.; Ma, Z.; Mahurin, S. M.; Jiao, J.; Hagaman, E. W.; Overbury, S. H.; Dai, S. *Catal. Lett.* **2008**, *121*, 209.
(74) Yan, W. F.; Mahurin, S. M.; Pan, Z. W.; Overbury, S. H.; Dai, S. *J. Am. Chem. Soc.* **2005**, *127*, 10480.
(75) Shou, M.; Takekawa, H.; Ju, D.-Y.; Hagiwara, T.; Lu, D.-L.; Tanaka, K. *Catal. Lett.* **2006**, *108*, 119.
(76) Zhu, H. G.; Ma, Z.; Overbury, S. H.; Dai, S. *Catal. Lett.* **2007**, *116*, 128.
(77) Yin, H. F.; Ma, Z.; Overbury, S. H.; Dai, S. *J. Phys. Chem. C* **2008**, *112*, 8349.
(78) Yin, H. F.; Wang, C.; Zhu, H. G.; Overbury, S. H.; Sun, S. H.; Dai, S. *Chem. Commun.* **2008**, 4357.
(79) Yu, H.; Chen, M.; Rice, P. M.; Wang, S. X.; White, R. L.; Sun, S. H. *Nano Lett.* **2005**, *5*, 379.
(80) Baiker, A.; Gasser, D.; Lenzner, J.; Reller, A.; Schlögl, R. *J. Catal.* **1990**, *126*, 555.
(81) Schlögl, R.; Loose, G.; Wesemann, M.; Baiker, A. *J. Catal.* **1992**, *137*, 139.
(82) Baiker, A. In *Preparation of Solid Catalysts*; Ertl, G., Knözinger, H., Weitkamp, J., Eds.; Wiley-VCH: Weinheim, 1999; p 43.
(83) Yu, K.; Wu, Z. C.; Zhao, Q. R.; Li, B. X.; Xie, Y. *J. Phys. Chem. C* **2008**, *112*, 2244.
(84) Dawood, F.; Leonard, B. M.; Schaak, R. E. *Chem. Mater.* **2007**, *19*, 4545.

JP811411Y